Multichannel fluctuating field approach to competing instabilities in interacting electronic systems

E. Linnér,[1] A. I. Lichtenstein,[2,3,4] S. Biermann,[1,5,6,7] and E. A. Stepanov[1]

[1]*CPHT, CNRS, École Polytechnique, Institut Polytechnique de Paris, 91120 Palaiseau, France*
[2]*I. Institute of Theoretical Physics, University of Hamburg, Jungiusstrasse 9, 20355 Hamburg, Germany*
[3]*European X-Ray Free-Electron Laser Facility, Holzkoppel 4, 22869 Schenefeld, Germany*
[4]*The Hamburg Centre for Ultrafast Imaging, Luruper Chaussee 149, 22761 Hamburg, Germany*
[5]*Collège de France, 11 place Marcelin Berthelot, 75005 Paris, France*
[6]*Department of Physics, Division of Mathematical Physics, Lund University, Professorsgatan 1, 22363 Lund, Sweden*
[7]*European Theoretical Spectroscopy Facility, 91128 Palaiseau, France*

(Received 12 October 2022; revised 21 February 2023; accepted 30 June 2023; published 24 July 2023)

Systems with strong electronic Coulomb correlations often display rich phase diagrams exhibiting different ordered phases involving spin, charge, or orbital degrees of freedom. The theoretical description of the interplay of the corresponding collective fluctuations giving rise to this phenomenology, however, remains a tremendous challenge. Here, we introduce a multichannel extension of the recently developed fluctuating field approach to competing collective fluctuations in correlated electron systems. The method is based on a variational optimization of a trial action that explicitly contains the order parameters of the leading fluctuation channels. It gives direct access to the free energy of the system, facilitating the distinction between stable and metastable phases of the system. We apply our approach to the extended Hubbard model in the weak to intermediate coupling regime where we find it to capture the interplay of competing charge density wave and antiferromagnetic fluctuations with qualitative agreement with more computationally expensive methods. The multichannel fluctuating field approach thus offers a promising route for a numerically low-cost treatment of the interplay between collective fluctuations in small to large systems.

DOI: 10.1103/PhysRevB.108.035143

I. INTRODUCTION

A hallmark of materials with strong electronic Coulomb correlations are their typically extremely rich phase diagrams, exhibiting various kinds of ordering phenomena. These result from competing instabilities involving, e.g., charge, spin, orbital, or pairing fluctuations. The theoretical description of these collective phenomena remains a challenging issue of computational complexity [1,2] as well as conceptual difficulty, e.g., the explicit breaking of symmetries [3,4]. In this sense, the interplay of competing electronic fluctuations constitutes a roadblock to the understanding of the complex phase diagrams of a wide range of material systems. Constructing simplified methods to study interplaying collective fluctuations is thus of crucial importance.

The extended Hubbard model [5–8] provides a suitable framework for investigating the interplay between collective electronic fluctuations. The physics of this model is determined by the competition between the local U and the nonlocal V Coulomb interactions. A repulsive U stabilizes collective spin fluctuations [9], which may compete with charge fluctuations driven by a strong repulsive V [10,11]. The earliest considerations of the extended Hubbard model were already implicit in the initial work of Hubbard in 1963 [5]. However, the first studies of the model occurred in the 1970s, with studies of the strong [10,12] and weak coupling limits of the half-filled one-dimensional (1D) chain [13,14]. Together with an access to the intermediate coupling regime by early numerical exact diagonalization and lattice Monte Carlo calculations [15,16], the phase diagram of the 1D extended Hubbard model was predicted to be composed of regions of strong charge density wave (CDW) and antiferromagnetic (AFM) fluctuations, with a CDW-AFM transition occurring in the vicinity of $U = 2V$. The transition was later discovered to be modified in the weak coupling limit by an intermediate bond-order wave (BOW) state [17,18], also arising in the ionic Hubbard model [19–22].

Extensive studies have been conducted on the extended Hubbard model for elucidating the interplay between collective charge and spin fluctuations [12,14–16,23–32]. Considerable insight has been acquired for the extended Hubbard model on a two-dimensional square lattice at half filling with nearest-neighbor interaction V [24–30,33–41], which we study in this paper. It has been found that this model displays a phase diagram similar to the 1D counterpart, besides the apparent lack of an intermediate BOW phase. In particular, the system reveals a checkerboard CDW pattern, which interplays with strong AFM fluctuations in the vicinity of a CDW-AFM transition line $U = 4V$ [24,42]. In a recent work [29] based on the dynamical cluster approximation (DCA) [43–45], the competition near the transition line has been shown to induce a coexistence region of charge- and spin-ordered states.

By the Mermin-Wagner theorem [46–48], magnetic ordering at finite temperatures is excluded in a broad class of one- and two-dimensional systems, including the extended Hubbard model, due to the continuous nature of the underlying symmetry. Thus, the regime of strong collective AFM fluctuations is, strictly speaking, not a phase. However, in this

paper the AFM phase will refer to a slightly broader definition of short-range AFM ordering, which transforms to a true phase for a quasi-two-dimensional system. In contrast, the discrete symmetry of the CDW allows for a true phase transition. In addition, technically speaking, in the present paper, we are performing calculations for finite systems, where long-range fluctuations are eventually cut off, so neither the AFM or CDW state are, strictly speaking, phases. Nevertheless, in the following, we will refer to both states as phases, since we are interested in the interplay of the competing fluctuations corresponding to these orderings. Our conclusions should thus be understood as applying either to finite systems, replacing the notion of the phase by a state dominated by the respective fluctuations, or to a quasi-two-dimensional system in the thermodynamic limit.

Limitations in the treatment of competing collective fluctuations arise in the currently available approaches employed for studying quantum lattice systems. Numerically exact methods, such as exact diagonalization [1] and lattice Monte Carlo [2] have studied the interplay between U and V [15,16,24,25] but are restricted to small system sizes and thus cannot address long-range collective fluctuations. The same problem is also inherent in cluster extensions of the dynamical mean-field theory (DMFT) [49–54], such as, e.g., DCA [43–45]. Diagrammatic methods based on the parquet approximation [55–60] allow one to account for the interplay between charge and spin fluctuations [30] originating from the two-particle vertex functions in an unbiased and powerful fashion. These vertices are incorporated with full momentum and frequency dependence, and the approach is thus computationally very expensive, which severally limits its applicability. Advanced diagrammatic extensions of DMFT [61] are able to describe long-range fluctuations simultaneously in different instability channels. In the presence of the nonlocal interaction V, this can be done within the dual boson theory [38,40,62–64], the dynamical vertex approximation (DΓA) [65,66], the triply irreducible local expansion (TRILEX) method [67], or the dual TRILEX (D-TRILEX) approach [31,32,68]. However, these fluctuations are usually treated in a ladderlike approximation, where different instability channels affect each other only indirectly via self-consistent renormalization of single- and two-particle quantities.

Current approaches to quantum lattice systems that are able to capture competing collective fluctuations are too complicated for broad usage. In this paper, we develop a multichannel generalization of the fluctuating field (FF) approach that allows us to incorporate multiple collective fluctuation channels and their interplay in a numerically cheap way without explicitly breaking the symmetry of the model. The FF method was originally introduced for the study of spin fluctuations in the classical Ising plaquettes [69,70] and was further developed for single- and multimode treatment of collective spin fluctuations in the Hubbard model [71–73]. We employ the proposed multichannel fluctuating field (MCFF) approach to study the interplay between CDW and AFM fluctuations in the extended Hubbard model on a half-filled square lattice with a repulsive on-site U and nearest-neighbor V interactions. We show that the MCFF approach predicts results for the CDW and AFM phase boundaries in qualitative agreement with more elaborate numerical methods. Furthermore, it allows us to model competing collective fluctuations from small systems to large systems near the thermodynamic limit. Importantly, the method is especially appropriate for small plaquettes, with relevance in small physical systems, e.g., molecular magnets [74–76], and due to conventional strongly correlated methods being commonly limited to small system sizes. In addition, the method is able to distinguish between stable and metastable (MS) collective fluctuations. For this reason, the MCFF approach allows us to capture the true ground state of the coexistence region of CDW and AFM fluctuations that was obtained in Ref. [29] on the basis of DCA calculations.

II. MODEL

For simplicity, our considerations are limited to a single-band extended Hubbard model. However, we note that our approach can be straightforwardly generalized to more complex single- and multiband quantum lattice systems. The Hamiltonian of the extended Hubbard model has the following form:

$$\hat{H} = -t \sum_{\langle i,j\rangle,\sigma} \hat{c}^{\dagger}_{i\sigma}\hat{c}_{j\sigma} + U \sum_{i} \hat{n}_{i\uparrow}\hat{n}_{i\downarrow} + \frac{V}{2} \sum_{\langle i,j\rangle,\sigma\sigma'} \hat{n}_{i\sigma}\hat{n}_{j\sigma'}. \quad (1)$$

In this expression, $\hat{c}^{(\dagger)}_{i\sigma}$ operators correspond to annihilation (creation) of electrons, where the subscripts denote the position i and spin projection $\sigma \in \{\uparrow, \downarrow\}$. Our system is modeled by the hopping t between nearest-neighbor sites $\langle i, j\rangle$ on a two-dimensional square lattice, with $t = 1$ being employed in this paper. The Coulomb interaction between electronic densities $\hat{n}_{i\sigma} = \hat{c}^{\dagger}_{i\sigma}\hat{c}_{i\sigma}$ contains the on-site U and the nearest-neighbor V components.

The extended Hubbard model Eq. (1) displays two symmetries of fundamental importance for our considerations: a continuous SU(2) symmetry associated with spin degrees of freedom and a discrete particle-hole symmetry related to charge degrees of freedom. To facilitate our later treatments, we include a sketch of the finite temperature U, V phase diagram of the extended Hubbard model on the two-dimensional square lattice in Fig. 1. Within the sketch, we denote the regime of strong CDW fluctuations (red gradient), with asymptotics of the CDW phase boundary highlighted, and the regime of strong AFM fluctuations (blue gradient). The CDW phase boundary occurs along $V = U/8 + \text{cst}$ at weak coupling [37], which transforms to $V = U/4$ at intermediate coupling [24], followed by $V \sim U + \text{cst}$ at strong coupling [33,38,40,62,77,78]. At weak coupling, the AFM phase boundary starts at a critical U, which further extends to the $V = U/4$ phase boundary at intermediate coupling [29]. We restrict our consideration to the weak to intermediate coupling regime, with the strong coupling regime being outside the scope of this paper.

The MCFF approach to be introduced in the next section is based on a variational principle conveniently formulated within the action formalism. Thus, it is suitable to rewrite the extended Hubbard model Eq. (1) in the form of the action,

$$\mathcal{S} = -\frac{1}{\beta N} \sum_{\mathbf{k},\nu,\sigma} c^{*}_{\mathbf{k}\nu\sigma} \mathcal{G}^{-1}_{\mathbf{k}\nu} c_{\mathbf{k}\nu\sigma} + \frac{U}{\beta N} \sum_{\mathbf{q},\omega} \rho_{\mathbf{q}\omega\uparrow}\rho_{-\mathbf{q},-\omega\downarrow} + \frac{1}{2\beta N} \sum_{\mathbf{q},\omega,\sigma\sigma'} V_{\mathbf{q}}\rho_{\mathbf{q}\omega\sigma}\rho_{-\mathbf{q},-\omega\sigma'}, \quad (2)$$

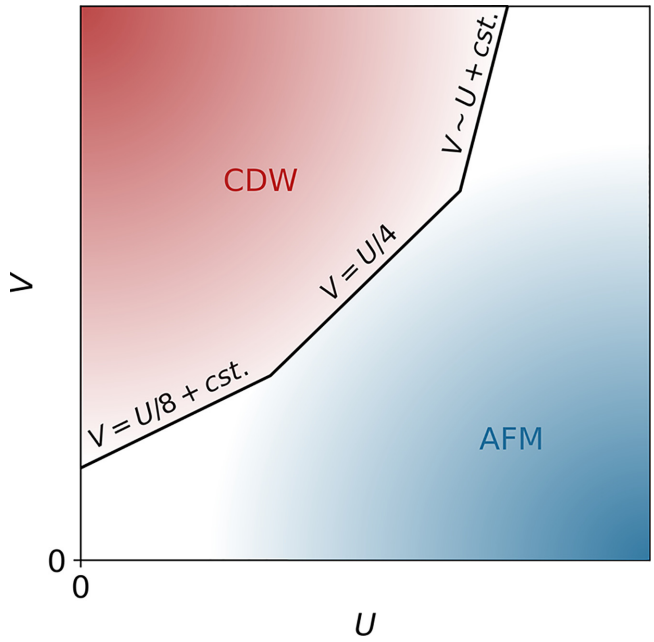

FIG. 1. Sketch of the phase diagram of the quasi-two-dimensional half-filled extended Hubbard model with repulsive interactions U and V at sufficiently low, but finite, temperature, allowing for antiferromagnetic (AFM) and charge density wave (CDW) fluctuations. Beyond a critical local interaction, a regime of dominant AFM fluctuations is expected, while strong nonlocal interactions drive the system into a CDW phase. At low U, V the orderings give way for a normal metal phase. The schematic phase boundaries of the CDW phase are determined by the asymptotic expressions $V = U/8 + \text{cst}$ at weak coupling [37], $V = U/4$ at intermediate coupling [24,25,42], and $V \simeq U + \text{cst}$ at strong coupling [33,38,40,62,77,78]. At weak to intermediate coupling, the AFM regime extrapolates from a critical U at vanishing V to the $V = U/4$ phase boundary [29].

with the inverse temperature β and number of sites N. Grassmann variables $c^{(*)}$ correspond to the annihilation (creation) of electrons, where the subscripts denote the momentum $\mathbf{k}$ and fermionic Matsubara frequency ν. The inverse of the bare (noninteracting) Green's function is defined as $\mathcal{G}^{-1}_{\mathbf{k}\nu} = i\nu + \mu - \epsilon_{\mathbf{k}}$, where μ is the chemical potential and $\epsilon_{\mathbf{k}} = -2(\cos k_x + \cos k_y)$ is the dispersion relation for the nearest-neighbor hopping on a two-dimensional square lattice. For convenience, the interaction parts of the action Eq. (2) are written in terms of the shifted densities $\rho_{\mathbf{q}\omega\sigma} = n_{\mathbf{q}\omega\sigma} - \langle n_{\mathbf{q}\omega\sigma}\rangle \delta_{\mathbf{q},\mathbf{0}}\delta_{\omega,0}$, where $\mathbf{q}$ and ω are the momentum and bosonic Matsubara frequency indices, respectively. This choice of shift will be argued for in our later derivation. In our considerations, the momentum-space representation for the nonlocal interaction follows $V_{\mathbf{q}} = 2V(\cos q_x + \cos q_y)$, as it is limited to only a nearest-neighbor interaction.

III. MULTICHANNEL FLUCTUATING FIELD THEORY

In this section, we derive a multichannel generalization of the FF theory that was originally introduced to address the fluctuations in a single (magnetic) channel [69,71–73]. We derive the MCFF theory by utilizing a variational approach formulated in Ref. [71], which allows us to incorporate the leading instabilities of the collective fluctuations.

A. Definition of trial action

We define a MCFF trial action

$$\mathcal{S}^* = -\frac{1}{\beta N}\sum_{\mathbf{k},\nu,\sigma} c^*_{\mathbf{k}\nu\sigma}\mathcal{G}^{-1}_{\mathbf{k}\nu}c_{\mathbf{k}\nu\sigma} + \sum_{\mathbf{Q},\varsigma}\left[\phi^\varsigma_{\mathbf{Q}}\rho^\varsigma_{-\mathbf{Q}} - \frac{1}{2}\frac{\beta N}{J^\varsigma_{\mathbf{Q}}}\phi^\varsigma_{\mathbf{Q}}\phi^\varsigma_{-\mathbf{Q}}\right] \tag{3}$$

that explicitly considers sets of scalar charge ($\varsigma = c$) and vector spin ($\varsigma = s \in \{x, y, z\}$) fields $\phi^\varsigma_{\mathbf{Q}}$ coupled to the composite variables $\rho^\varsigma_{\mathbf{Q}} = n^\varsigma_{\mathbf{Q}} - \langle n^\varsigma_{\mathbf{Q}}\rangle\delta_{\mathbf{Q},\mathbf{0}}$ associated with the respective static ($\omega = 0$) order parameters of interest. Here

$$n^\varsigma_{\mathbf{Q}} = \frac{1}{\beta N}\sum_{\mathbf{k},\nu,\sigma\sigma'} c^*_{\mathbf{k}+\mathbf{Q},\nu\sigma}\sigma^\varsigma_{\sigma\sigma'}c_{\mathbf{k}\nu\sigma'}, \tag{4}$$

where $\mathbf{Q}$ is the ordering wave vector, σ^c is the identity, and σ^s are the Pauli spin matrices. The interaction part of the trial action Eq. (3) contains a set of stiffness constants $J^\varsigma_{\mathbf{Q}}$ that will be determined. Within the approach, the aim is to incorporate the set of classical fields associated with the main leading instabilities of the system. Importantly, the form of the MCFF trial action Eq. (3) is identical to a Hubbard-Stratonovich action. As the Hubbard-Stratonovich transformation is an exact rewriting of the fermionic action through the introduction of additional auxiliary bosonic degrees of freedom, the MCFF theory would be exact if all modes in quasimomentum and frequency space were treated explicitly. However, in practice, the MCFF theory is restricted to only the main leading instabilities of the system, allowing for a numerically low-cost treatment. Limited to only a few modes, the MCFF theory will appear to converge in the thermodynamic limit to a symmetry-conserving sum over the symmetry-broken solutions of mean-field theory. However, for any finite system, the MCFF theory will introduce important corrections beyond mean-field theory.

B. Integrating out fermionic degrees of freedom

The trial action Eq. (3) has a Gaussian form with respect to the Grassmann variables $c^{(*)}$ and classical fields ϕ^ς. This allows one to obtain an effective action for either fermionic or classical degrees of freedom by analytically integrating out the other degrees of freedom. Integrating out the fermionic degrees of freedom, the effective action for the classical fields becomes

$$\mathcal{S}_\phi = -\operatorname{Tr}\ln\left[\mathcal{G}^{-1}_{\mathbf{k}\nu}\delta_{\mathbf{Q},0}\delta_{\sigma,\sigma'} - \sum_\varsigma \phi^\varsigma_{\mathbf{Q}}\sigma^\varsigma_{\sigma\sigma'}\right] - \frac{1}{2}\sum_{\mathbf{Q},\varsigma}\frac{\beta N}{J^\varsigma_{\mathbf{Q}}}\phi^\varsigma_{\mathbf{Q}}\phi^\varsigma_{-\mathbf{Q}}. \tag{5}$$

The trace is taken over the momenta $\mathbf{k}$, $\mathbf{Q}$, frequency ν, and spin σ, σ' indices. The effective action Eq. (5) depends on a small number of classical fields $\phi^\varsigma_{\mathbf{Q}}$. For this reason, the phase

diagram that captures the interplay between the different FFs can be studied by means of the free energy $\mathcal{F}_\phi$ corresponding to this action. Importantly, $\mathcal{F}_\phi$ nonperturbatively incorporates the fluctuations of the relevant order parameters $\rho^\varsigma_{\mathbf{Q}}$ by allowing the global minimum of $\mathcal{F}_\phi$ to shift away from $\phi^\varsigma_{\mathbf{Q}} = 0$.

C. Determination of the stiffness parameters via a variational principle

To determine $J^\varsigma_{\mathbf{Q}}$, we use the Peierls-Feynman-Bogoliubov variational principle [79–81], as previously employed for the single-mode FF method [71]. This variational principle allows one to construct a unique and unambiguous set of $J^\varsigma_{\mathbf{Q}}$ which minimizes the functional

$$\mathcal{F}\big(J^\varsigma_{\mathbf{Q}}\big) = \mathcal{F}_c\big(J^\varsigma_{\mathbf{Q}}\big) + \frac{1}{\beta N}\langle \mathcal{S} - \mathcal{S}_c\rangle_{\mathcal{S}_c} \tag{6}$$

by varying $J^\varsigma_{\mathbf{Q}}$. Here, $\langle\cdots\rangle_{\mathcal{S}_c}$ denotes the expectation value with respect to the effective fermionic action $\mathcal{S}_c$, corresponding to the trial action Eq. (3) with the classical fields $\phi^\varsigma_{\mathbf{Q}}$ being integrated out:

$$\mathcal{S}_c = -\frac{1}{\beta N}\sum_{\mathbf{k},\nu,\sigma} c^*_{\mathbf{k}\nu\sigma}\mathcal{G}^{-1}_{\mathbf{k}\nu}c_{\mathbf{k}\nu\sigma} + \frac{1}{2}\sum_{\mathbf{Q},\varsigma}\frac{J^\varsigma_{\mathbf{Q}}}{\beta N}\rho^\varsigma_{\mathbf{Q}}\rho^\varsigma_{-\mathbf{Q}}. \tag{7}$$

In addition, we have introduced the free energy $\mathcal{F}_c(J^\varsigma_{\mathbf{Q}}) = -\ln(\mathcal{Z}_c)/\beta N$, where $\mathcal{Z}_c$ is the partition function of the action $\mathcal{S}_c$. We finally note that writing the initial Eq. (2) and the trial Eq. (3) actions in terms of ρ^ς variables above allows us to keep the bare Green's function $\mathcal{G}_{\mathbf{k}\nu}$ identical in both actions, simplifying the variational treatment. In contrast, another choice of variables would necessitate a shift in the chemical potential in the trial action $\mathcal{S}^*$ relative to the extended Hubbard action $\mathcal{S}$.

For the evaluation of $\langle\cdots\rangle_{\mathcal{S}_c}$, we explicitly rewrite the expectation value as (see Ref. [71] for details)

$$\langle\cdots\rangle_{\mathcal{S}_c} = \langle\langle\cdots\rangle_{\mathcal{S}_e}\rangle_{\mathcal{S}_\phi}, \tag{8}$$

where the inner expectation value is taken with respect to the fermionic part of the trial action Eq. (3),

$$\mathcal{S}_e = -\frac{1}{\beta N}\sum_{\mathbf{k},\nu,\sigma} c^*_{\mathbf{k}\nu\sigma}\mathcal{G}^{-1}_{\mathbf{k}\nu}c_{\mathbf{k}\nu\sigma} + \sum_{\mathbf{Q},\varsigma}\phi^\varsigma_{\mathbf{Q}}\rho^\varsigma_{-\mathbf{Q}}, \tag{9}$$

which depends on the classical fields $\phi^\varsigma_{\mathbf{Q}}$. A useful property of the inner expectation value is that Wick's theorem applies, as $\mathcal{S}_e$ is a Gaussian action with respect to the fermions. Note that for any nonzero value of the classical field $\phi^\varsigma_{\mathbf{Q}}$, the term $\phi^\varsigma_{\mathbf{Q}}\rho^\varsigma_{-\mathbf{Q}}$ in the action Eq. (9) allows for the collective fluctuations by breaking the associate symmetries in the $\mathcal{S}_e$ subsystem. The symmetries of the full system $\mathcal{S}_c$ are, however, retained by ultimately taking the outer expectation value $\langle\cdots\rangle_{\mathcal{S}_\phi}$. We emphasize that mean-field approaches require the introduction of an explicit symmetry breaking in the system to enter ordered phases. In contrast, the FF approach allows the system to fluctuate in an ordering channel while retaining the underlying symmetry without any explicit symmetry breaking.

In this paper, we limit our considerations to the collective AFM and CDW fluctuations with the $\mathbf{Q} = (\pi, \pi)$ wave vector that are the leading modes in the half-filled extended Hubbard model. Our choice to keep only the main $\mathbf{Q}$ mode for each fluctuation is motivated by the observation that the momentum-space representation for the static lattice susceptibility $X^\varsigma(\mathbf{q}, \omega = 0)$ at the transition point between the normal and the ordered phases usually has the form of a delta-function-like Bragg peak located at the ordering vectors $X^\varsigma(\mathbf{q}, \omega = 0) \sim \delta_{\mathbf{q},\mathbf{Q}}$ (see, e.g., Refs. [31,32]). Thus (while a multimode FF has been developed to incorporate the leading and subleading momentum modes in Ref. [72]), we argue that considering only the leading $\mathbf{Q}$ mode is sufficient for predicting phase boundaries in the case of strong competing fluctuations.

Given the symmetries of the considered model, the charge and spin channels are described by two independent stiffness constants $J^s_{\mathbf{Q}}$ and $J^c_{\mathbf{Q}}$ that can be obtained by minimizing the corresponding free energy Eq. (6) as

$$\frac{\partial\mathcal{F}\big(J^\varsigma_{\mathbf{Q}}\big)}{\partial J^\varsigma_{\mathbf{Q}}} = 0. \tag{10}$$

This leads to $J^s_{\mathbf{Q}} = -U/2$ for the stiffness constant in the spin channel, in agreement with the result of the previous work [71], and to $J^c_{\mathbf{Q}} = U/2 - 4V$ in the charge channel (see Appendix A for details). Importantly, the employed variational approach avoids the hidden Fierz ambiguity in the decoupling of the on-site Coulomb interaction U between the different fluctuating channels [82–84]. In this regard, it is interesting to note that the obtained values of the stiffness constants $J^\varsigma_{\mathbf{Q}}$ correspond to the form of the bare interaction in Hartree-Fock theory, which avoids the Fierz ambiguity problem [42,85], and in the fluctuating exchange (FLEX) approximation [58,59]. In addition, the stiffness constants $J^\varsigma_{\mathbf{Q}}$ are in agreement with the diagrammatic D-TRILEX approach, which resolves the Fierz ambiguity problem in a completely different way [68,86,87]. At this step, the effective action Eq. (5) is fully defined and can be solved numerically exactly, which allows the approach to respect the underlying symmetry of the system and, in addition, incorporate non-Gaussian fluctuations nonperturbatively, as will be conducted below.

D. Free energy

In this section, we describe the method employed to investigate the interplay between collective CDW and AFM fluctuations in the extended Hubbard model using the developed MCFF method. The phase diagram of the system can be determined based on the free energy $\mathcal{F}_\phi$ of the effective MCFF action Eq. (5), which allows us to avoid computing the more complex susceptibilities in the instability channels. To find the phase boundary for the CDW phase, we introduce the free energy $\mathcal{F}(\phi^c_{\mathbf{Q}})$ for the respective classical field $\phi^c_{\mathbf{Q}}$ by integrating out the spin degrees of freedom $\phi^s_{\mathbf{Q}}$ numerically exactly:

$$\mathcal{F}\big(\phi^c_{\mathbf{Q}}\big) = -\frac{1}{\beta N}\ln\int D\big[\phi^s_{\mathbf{Q}}\big]\,\exp\big\{-\mathcal{S}_\phi\big[\phi^c_{\mathbf{Q}}, \phi^s_{\mathbf{Q}}\big]\big\}. \tag{11}$$

Within the logarithm, the numerical integration over $\phi^s_{\mathbf{Q}}$ may be performed by the trapezoidal rule over a sufficiently dense grid, exploiting the rotational invariance of the action $\mathcal{S}_\phi[\phi^c_{\mathbf{Q}}, \phi^s_{\mathbf{Q}}]$ with respect to $\phi^s_{\mathbf{Q}}$. The first term in the action Eq. (5) can be efficiently evaluated by rewriting the trace over all internal indices as a trace over $\mathbf{k}$ and ν indices

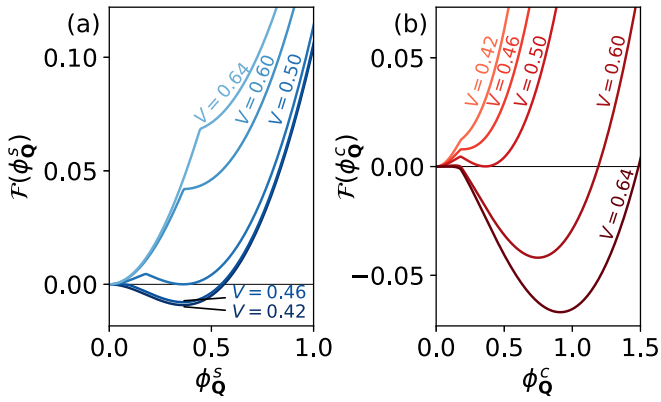

FIG. 2. Free energy $\mathcal{F}(\phi^{\varsigma}_{\mathbf{Q}})$ for the spin (a) and charge (b) channels. The results are obtained for the half-filled extended Hubbard model on a square lattice at $\beta = 10$ and $U = 2$ in the vicinity of the CDW-AFM transition point $V = U/4$ for a plaquette of 128×128 lattice sites. Choice of U, V is denoted as stars in Fig. 3.

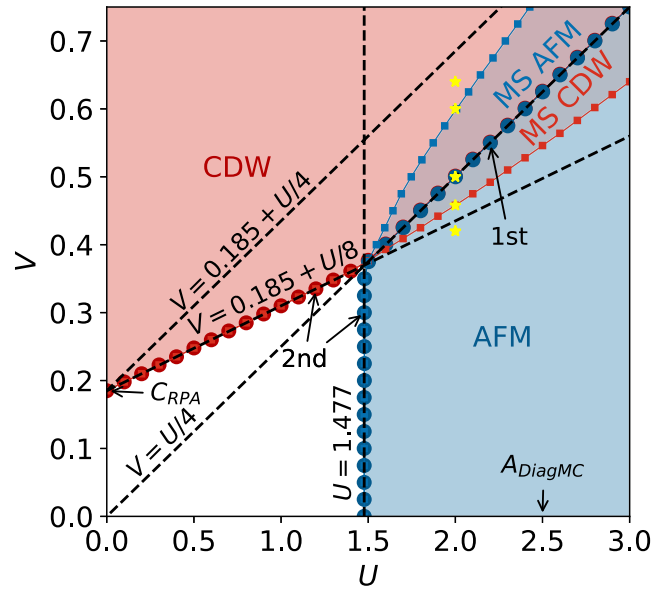

FIG. 3. Phase diagram for the half-filled extended Hubbard model with repulsive U, V interactions as predicted by the MCFF approach. The result is obtained at $\beta = 10$ for a plaquette of 128×128 lattice sites. Red and blue areas depict the CDW and AFM phases, respectively. The corresponding phase boundaries are shown by colored circles. Black dashed lines describe the asymptotic behavior of the phase boundaries: $V = 0.185 + U/8$ for CDW, $U = 1.477$ for AFM, and $V = U/4$ for CDW-AFM transitions. The boundaries of metastable CDW and AFM phases are illustrated by lines with small square markers. Metastability displays the first-order nature of the CDW-AFM phase transition to contrast with the second-order phase transitions occurring between the normal metal phase (white region) and the CDW and AFM phases. Yellow stars depict the points at which the free energies shown in Fig. 2 were calculated. For comparison, we add the RPA estimate $C_{\mathrm{RPA}} = 0.185$ for the CDW boundary in the $U \to 0$ limit, and the DiagMC estimate A_{DiagMC} for the AFM boundary in the limit of $V \to 0$ [88]. The RPA estimate $V = 0.185 + U/4$ for the CDW boundary is also shown.

over the logarithm of the determinant of a 4×4 matrix in a 2×2 momentum $(\mathbf{k}, \mathbf{k}+\mathbf{Q})$ and 2×2 spin $(\uparrow, \downarrow)$ space: $\mathrm{Tr}_{\mathbf{k},\mathbf{Q},\nu,\sigma} \ln[\cdots] = \mathrm{Tr}_{\mathbf{k},\nu} \ln \det_{\mathbf{Q},\sigma}[\cdots]$. Note that within this rewriting, $\mathrm{Tr}_{\mathbf{k}}$ is taken over the reduced (half) Brillouin zone. The sum over the Matsubara frequencies ν is performed analytically, leaving the $\mathbf{k}$ summation to be performed numerically. The free energy of the classical vector spin field $\phi^s_{\mathbf{Q}}$ can be obtained in a similar way by integrating out the $\phi^c_{\mathbf{Q}}$ field. This procedure allows us to construct the free energy for a single channel that, however, fully accounts for the effect of collective fluctuations in the other channel that is integrated out. The introduced free energy has the stability requirement $J^{\varsigma}_{\mathbf{Q}} < 0$ that ensures that $\mathcal{F}(\phi^{\varsigma})$ has a global minimum for each ϕ^{ς}, i.e., the $\phi^{\varsigma}_{\mathbf{Q}}$ mode is stable. In contrast, the effective fermionic action Eq. (7) for $J^{\varsigma}_{\mathbf{Q}} > 0$ is associated with an unstable collective mode, as ordering in the $\rho^{\varsigma}_{\mathbf{Q}}$ channel is energetically penalized. This requirement limits the regions in which the different collective fluctuations are incorporated within the MCFF scheme. For the considered extended Hubbard model, the stability requirement for the AFM and CDW fluctuations are $U > 0$ and $V > U/8$, respectively. With the method for constructing the free energy within the MCFF theory, we may now finally generate the U, V phase diagram for the extended Hubbard model.

IV. RESULTS

A. Phase diagram in the thermodynamic limit

We now focus on the half-filled extended Hubbard model on a square lattice with repulsive U and V interactions. The numerical MCFF investigation is based on the construction of the free energies Eq. (11) for the CDW and AFM fluctuations. A typical behavior of the introduced free energy $\mathcal{F}(\phi^{\varsigma}_{\mathbf{Q}})$ is illustrated in Fig. 2. In the normal phase, the global minimum of $\mathcal{F}(\phi^{\varsigma}_{\mathbf{Q}})$ lies at $\phi^{\varsigma}_{\mathbf{Q}} = 0$. The formation of the ordered phase is signaled by a shift of the global minimum to a $\phi^{\varsigma}_{\mathbf{Q}} \neq 0$ point. In addition to the global minimum, the free energy may reveal a local minimum that indicates the presence of a MS phase. We will discuss the appearance of the MS phases below. Finally, we observe a nonanalyticity appearing as a kink in the free energy $\mathcal{F}(\phi^{\varsigma}_{\mathbf{Q}})$. It signals a change of behavior of $\mathcal{F}(\phi^{\varsigma}_{\mathbf{Q}})$ between the region in the vicinity of $\phi^{\varsigma}_{\mathbf{Q}} = 0$, where the fluctuations in the integrated channel are strong, and the region of $\phi^{\varsigma}_{\mathbf{Q}} \neq 0$, where the fluctuations in the considered channel are strong. Thus, the observed kink is inherently connected to the interplay between the collective CDW and AFM fluctuations.

We perform calculations for a plaquette of 128×128 lattice sites with periodic boundary conditions, which can arguably be considered as the thermodynamic limit, as we do not see any difference in the results compared to the 256×256 case. Figure 3 shows the phase diagram of the system obtained at $\beta = 10$. We note that the MCFF method can also be applied at much lower temperatures. The choice of β is due to convenience in comparison to earlier works. Based on the free-energy considerations discussed above, our calculations reveal three phases: a normal (white color), a CDW (red color), and an AFM (blue color) phase. We find that in the weak coupling regime $U \leqslant 1.447$, the CDW phase boundary follows the $V = 0.185 + U/8$ line. This result is in exact

agreement with the perturbative estimation $V = C_{\mathrm{RPA}} + U/8$ [37], where the constant C_{RPA} corresponds to the critical value of the nonlocal interaction for the CDW transition $V^{\mathrm{CDW}}_{U=0}$ obtained for $U = 0$ using the random phase approximation (RPA). The RPA estimate is determined by the critical $V^{\mathrm{CDW}}_{U=0}$ associate with a singularity in the RPA construction of the charge susceptibility at the (π, π) point or equivalently determined by a vanishing RPA dielectric function. For the considered system, $C_{\mathrm{RPA}} = 0.1847$, which confirms that the MCFF theory correctly captures the exact $U \to 0$ limit for the CDW phase boundary. The AFM phase boundary in the weak coupling regime lies along the $U = 1.477$ line in exact agreement with the FLEX result obtained for $V = 0$: $A_{\mathrm{FLEX}} = U^{\mathrm{AFM}}_{V=0} = 8C_{\mathrm{RPA}}$. However, FLEX is known to underestimate the critical interaction for the AFM transition. For instance, in the thermodynamic limit, the exact diagrammatic Monte Carlo (DiagMC) solution gives $A_{\mathrm{DiagMC}} \simeq 2.5$ for $\beta = 10$ [88]. Determination of $U^{\mathrm{AFM}}_{V=0}$ within FLEX is similar to the RPA estimate of the critical $V^{\mathrm{CDW}}_{U=0}$, associated instead with a divergence of the FLEX construction of the spin susceptibility at the (π, π) point. We note that in the weak-coupling regime close to the obtained phase boundaries, either the CDW or AFM fluctuation is negligibly small. If one neglects one of these two modes within the MCFF method and applies a saddle-point approximation to the remaining mode, the theory reduces to a mean-field approach with the form of the bare local interactions $U^{c/s} = \pm U/2$ used, e.g., in the FLEX approach. The exact agreement for the phase boundaries in the weak-coupling regime of the FF and mean-field theories can also be shown analytically (see Appendix B).

In the moderate interaction regime, where the competition between the CDW and AFM fluctuations is strong, one has to take both fluctuations into account. Indeed, if one considers fluctuations only in one channel and completely disregards the other channel, the single-channel FF method predicts the CDW and AFM phase boundary to follow exactly $V = C_{\mathrm{RPA}} + U/8$ and $U = 8C_{\mathrm{RPA}}$, respectively (see Appendix B), as depicted by dashed lines in Fig. 3. The single-channel FF method thus predicts the weak interaction estimate to continue into the moderate interaction regime. If we now consider both fluctuations, the CDW and AFM phases are mutually exclusive, with the interplay leading to the system developing a CDW-AFM phase boundary at $V = U/4$ in agreement with numerically exact techniques [24,25] and the mean-field Hartree-Fock estimate [42], and follows the mean-field RPA or *GW* [78] prediction $V = U/4 + \mathrm{cst}$ (except for a constant shift). An explanation for the simple form of the CDW-AFM phase boundary is rather intuitive. Due to both fluctuations displaying identical ordering vectors $\mathbf{Q}$, their contributions to the first term of the effective action Eq. (5) are analogous. Thus, the strength of these fluctuations is dominantly determined by the stiffness parameters: $J^s_{\mathbf{Q}} = -U/2$ and $J^c_{\mathbf{Q}} = U/2 - 4V$. An equivalence between the two stiffness parameters thus arises at $V = U/4$, i.e., along the CDW-AFM phase boundary. A more nontrivial competition arises for small system sizes as considered in the next section. In addition, nontrivial interplay may arise for competing modes characterized by different ordering vectors $\mathbf{Q}$, due to the coupling of modes through the first term of the effective action Eq. (5).

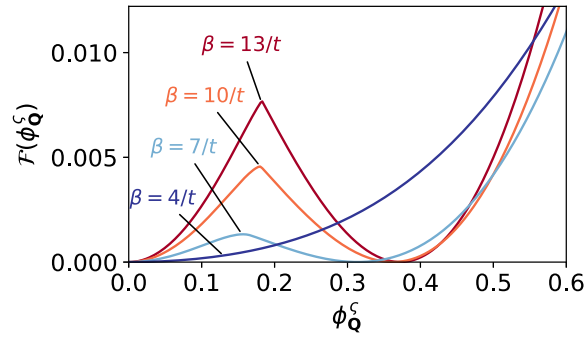

FIG. 4. Free energy $\mathcal{F}(\phi^c_{\mathbf{Q}}) = \mathcal{F}(\phi^s_{\mathbf{Q}})$ calculated at the CDW-AFM transition point $U = 2$, $V = 0.5$ for a plaquette of 128×128 lattice sites, with different values of the inverse temperature β.

Interestingly, we find that in some regions inside the CDW and AFM phases, besides the global minimum, the free energy $\mathcal{F}(\phi^\varsigma_{\mathbf{Q}})$ reveals a local minimum. The appearance of the local minimum can be associated with the presence of a MS phase. The boundaries of the MS phases are depicted in Fig. 3 by blue (MS AFM) and red (MS CDW) lines with small square markers. Figure 2 illustrates a particular example of the free energy behavior in the regime of strong competing CDW and AFM fluctuations. In the spin channel [Fig. 2(a)], as V is increased from deep within the AFM phase the global minimum at $\phi^s_{\mathbf{Q}} \neq 0$ in the free energy $\mathcal{F}(\phi^s_{\mathbf{Q}})$ turns into a local minimum above the CDW-AFM transition point $V = U/4$, where the CDW ordering becomes dominant. The local minimum disappears at the MS AFM phase transition point, which for $U = 2$ corresponds to $V = 0.60$. Similar results can be found for the charge channel [Fig. 2(b)]: As V decreases from deep within the CDW phase, the MS CDW phase appears at the AFM-CDW transition point and vanishes at $U = 2, V = 0.46$.

We note that at the CDW-AFM transition, the minima located at $\phi^\varsigma_{\mathbf{Q}} = 0$ and $\phi^\varsigma_{\mathbf{Q}} \neq 0$ points correspond to the same value of the free energy $\mathcal{F}(\phi^\varsigma_{\mathbf{Q}})$. On the contrary, no MS solution occurs in the vicinity of the phase boundaries that separate the normal phase from either the CDW or AFM phases. This result suggests that the transitions in the latter case are of second order, while the transition between the competing CDW and AFM phases is of first order. In addition, we find that the spin and charge channels are degenerate $[\mathcal{F}(\phi^s_{\mathbf{Q}}) = \mathcal{F}(\phi^c_{\mathbf{Q}})]$ along the CDW-AFM transition line, which indicates that the two instabilities are mutually exclusive. If these free energies were not identical at the transition point, one channel would be energetically favorable. Figure 4 shows the behavior of the free energy $\mathcal{F}(\phi^\varsigma_{\mathbf{Q}})$ at the CDW-AFM transition point $U = 2, V = 0.5$ for different temperatures. We observe that at high temperature corresponding to $\beta = 4$ the AFM and CDW fluctuations are suppressed, and the free energy has only one minimum at $\phi^\varsigma_{\mathbf{Q}} = 0$: the normal phase. Upon lowering the temperature, the second minima develops at $\phi^\varsigma_{\mathbf{Q}} \neq 0$ and propagates to larger values of $\phi^\varsigma_{\mathbf{Q}}$, corresponding to the increase of the strength of corresponding fluctuations. We also observe that the free-energy barrier between the two minima increases with decreasing temperature. A larger energy barrier allows for a more stable coexistence of the two phases associated with $\phi^\varsigma_{\mathbf{Q}} = 0$ and $\phi^\varsigma_{\mathbf{Q}} \neq 0$. It

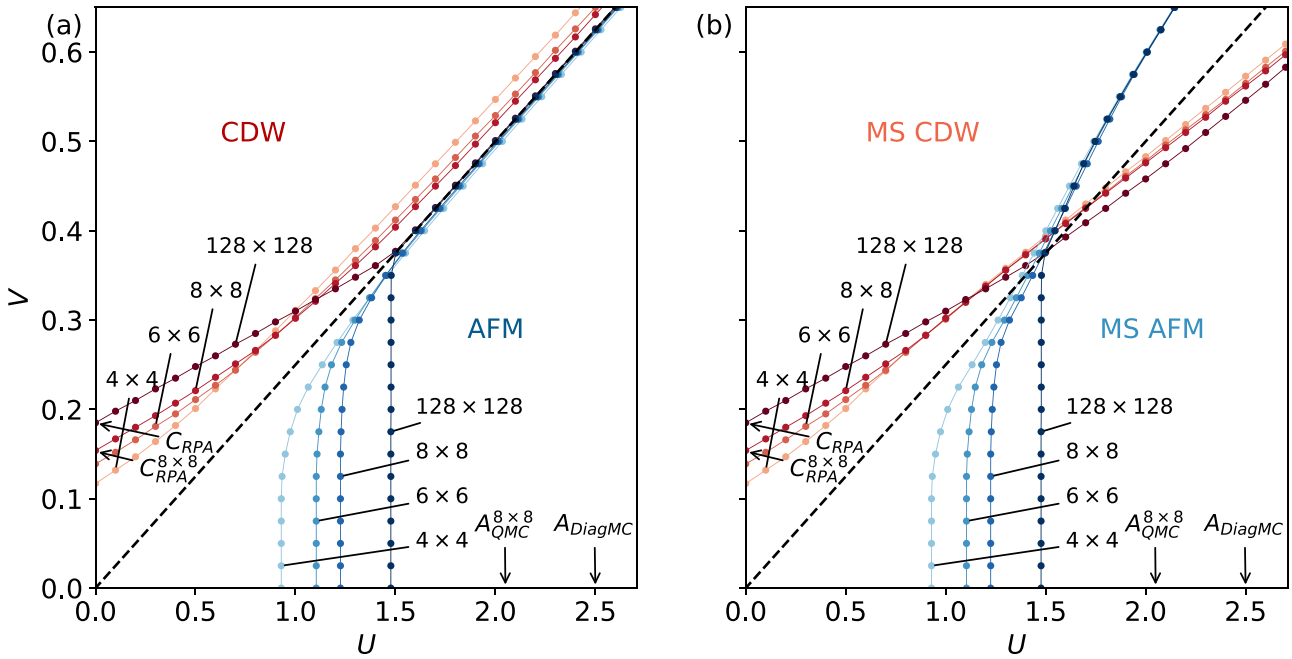

FIG. 5. Stable (a) and metastable (b) AFM (blue) and CDW (red) ordering boundaries predicted by the MCFF approach for the half-filled extended Hubbard model on 4×4, 6×6, 8×8, and 128×128 plaquettes at $\beta = 10$. The dashed line specifies the mean-field estimate for the CDW-AFM phase boundary $V = U/4$. For comparison, the RPA estimates C_{RPA} and $C^{8\times8}_{\mathrm{RPA}}$ for the CDW boundary in the $U \to 0$ in the thermodynamic limit and for a 8×8 plaquette, respectively, are included. In addition, the DiagMC estimate A_{DiagMC}, taken from Ref. [88], and the QMC estimate $A^{8\times8}_{\mathrm{QMC}}$ for the AFM boundary in the limit of $V \to 0$ are included in the thermodynamic limit and for a 8×8 plaquette, respectively.

should be emphasized, however, that the two channels are degenerate and that the minima at $\phi^{\zeta}_{\mathbf{Q}} = 0$ and $\phi^{\zeta}_{\mathbf{Q}} \neq 0$ have the same energy only at the CDW-AFM transition point. Away from this point, one of the two solutions becomes MS, which means that one of the CDW or AFM phases always dominates. Distinguishing between stable and MS solutions is not a trivial problem, and even the more elaborate DCA method in the regime of strong competing CDW and AFM fluctuations predicts a coexistence between these two mutually exclusive phases [29]. Thus, the ability to distinguish between the stable and the MS phases is an advantage of the MCFF method.

B. Evolution of the phase diagram with system size

The MCFF approach can also be applied to small systems, where it is expected to perform significantly better than the conventional mean-field theory [69,71]. For small system sizes, the result of the MCFF method can be compared to the exact Monte Carlo calculations. Figure 5 displays the stable (a) and MS (b) ordering boundaries for AFM and CDW phases for 4×4, 6×6, and 8×8 plaquettes, in addition to the previously considered 128×128 plaquette near the thermodynamic limit. For all system sizes, the MCFF approach extrapolates the AFM and CDW ordering boundaries between weak coupling results obtained, respectively, on the basis of FLEX calculations and perturbative estimations, and the asymptotic behavior of the CDW-AFM phase boundary at intermediate coupling predicted by mean-field theories. A region of coexisting stable and MS ordering is observed for all system sizes. Phase boundaries of the coexistence region appears converged for the 128×128 plaquette, indicating its stability in the thermodynamic limit. Importantly, we observe for small systems a more significant modification of the weak coupling CDW and AFM phase boundaries as predicted by the MCFF approach, due to the interplay of collective fluctuations. The modification displays itself by a bending of the phase boundaries not only in the vicinity of $V = U/4$, a distinct effect beyond conventional mean-field theory estimates.

To gain insight into the performance of the MCFF approach with inclusion of collective AFM and CDW fluctuations, we now perform a comparison with respect to numerically exact QMC simulations. For a 8×8 plaquette, QMC simulations give us $A^{8\times8}_{\mathrm{QMC}} = 2.05 \pm 0.05$ for $\beta = 10$. By a comparison to the MCFF prediction of $U^{\mathrm{AFM}}_{V=0} = 1.225$, we find a significant overestimation of the critical interaction U for the AFM phase boundary. This observation is consistent with our result for the 128×128 plaquette and can be related to dynamical correlation effects that are not incorporated within the approach. In contrast, the MCFF method accurately determines the CDW phase boundary at small U, with the MCFF prediction for the critical interaction $V^{\mathrm{CDW}}_{U=0}$ coinciding with the RPA result C_{RPA} for all plaquette sizes.

C. Measure of collective fluctuations

To quantify the strength of the collective fluctuations in the MCFF approach around the minimum of the free energy, we introduce $\langle |n^{\zeta}_{\mathbf{Q}}| \rangle$ as a measure. The measure $\langle |n^{\zeta}_{\mathbf{Q}}| \rangle$ is computed by taking the expectation value of $|n^{\zeta}_{\mathbf{Q}}|$ in the respective channel, i.e., performing a numerical integration over all classical field degrees of freedom associated with the collective fluctuations. The numerical integration corresponds

to the inclusion of fluctuations about the saddle point known to be important, e.g., see work on the crossover from BCS theory to Bose-Einstein condensate [89,90]. Our calculations of the measure $\langle|n^{\varsigma}_{\mathbf{Q}}|\rangle$ are compared to the saddle-point estimate $\langle|n^{\varsigma}_{\mathbf{Q}}|\rangle_{\mathrm{MF}}$, i.e., the value at the minimum of the free energy, which is equivalent with a conventional mean-field theory estimate. Thus, we seek to evaluate the differences between the FF and mean-field theories.

Figure 6 displays the calculated integrated measure $\langle|n^{\varsigma}_{\mathbf{Q}}|\rangle$ and the saddle-point measure $\langle|n^{\varsigma}_{\mathbf{Q}}|\rangle_{\mathrm{MF}}$, in addition to their difference $\langle|n^{\varsigma}_{\mathbf{Q}}|\rangle - \langle|n^{\varsigma}_{\mathbf{Q}}|\rangle_{\mathrm{MF}}$, at $\beta = 10$ for plaquettes of the size 4×4, 6×6, 8×8, and 128×128 along $V = U/4$. Specifically, within Figs. 6(a) and 6(b), the measures and their difference is calculated within the single-channel FF theory, namely, without considering the interplay between the fluctuations in the competing channel. Note that along $V = U/4$, the noninterplaying collective CDW and AFM fluctuations are degenerate. We observe $\langle|n^{\varsigma}_{\mathbf{Q}}|\rangle$, displayed as a solid line in Fig. 6(a), to monotonically increase as a function of U. The measure $\langle|n^{\varsigma}_{\mathbf{Q}}|\rangle$ vanishes in the limit of $U \to 0$ and saturates to the mean-field theory estimate $\langle|n^{\varsigma}_{\mathbf{Q}}|\rangle_{\mathrm{MF}}$ in the limit of large U, displayed as a dashed line in Fig. 6(a). We observe in Fig. 6(b) the deviation of the measure relative to the saddle-point estimate is positive and a monotonically increasing function of U below the phase boundaries evaluated within mean-field theory. A sharp decrease in the deviation follows above the phase boundaries, until a maximal negative deviation is reached, in turn followed by a saturation to zero deviation at large U. The collective fluctuations around the minimum of the free energy are most relevant in the vicinity of the phase transition, and especially for small systems. We observe the difference $\langle|n^{\varsigma}_{\mathbf{Q}}|\rangle_{\mathrm{MF}}$ to be suppressed with increasing system size. However, we note that for a plaquette of size 128×128, deviations with respect to mean-field theory remain small but non-negligible close to the phase boundary.

We now consider the measures for interplaying collective CDW and AFM fluctuations within the introduced MCFF theory, displayed in Figs. 6(c)–6(f). Due to degeneracy of the saddle-point minima of the CDW and AFM channels along $V = U/4$, two choices of $\langle|n^{\varsigma}_{\mathbf{Q}}|\rangle_{\mathrm{MF}}$ exist. Either $\langle|n^{c}_{\mathbf{Q}}|\rangle_{\mathrm{MF}}$ is nonzero for vanishing $\langle|n^{s}_{\mathbf{Q}}|\rangle_{\mathrm{MF}}$, or vice versa. We observe that the collective AFM fluctuations [Fig. 6(e)] dominate over the collective CDW fluctuations [Fig. 6(c)] in the regime of study. This naturally follows from the larger number of degrees of freedom of the AFM mode relative the CDW mode. A behavior similar to the single-channel results is observed in the measure $\langle|n^{s}_{\mathbf{Q}}|\rangle$, displayed as a solid line in Fig. 6(e). However, within the multichannel results the measure $\langle|n^{s}_{\mathbf{Q}}|\rangle$ is larger for the interplaying treatment due to the additional channel of fluctuation. In contrast, the measure $\langle|n^{c}_{\mathbf{Q}}|\rangle$ behaves dissimilar to the single-channel results. We observe the measure $\langle|n^{c}_{\mathbf{Q}}|\rangle$ to display a nonmonotonic behavior: increasing as a function of U at small U and decreasing as a function of U at large U. In fact, the measure $\langle|n^{c}_{\mathbf{Q}}|\rangle$ vanishes in both limits of small and large U. As noted previously, the largest deviation with respect to mean-field theory occurs in the vicinity of the phase transition and for small system sizes. In the thermodynamic limit, the collective CDW and AFM fluctuations appear to saturate to the mean-field theory,

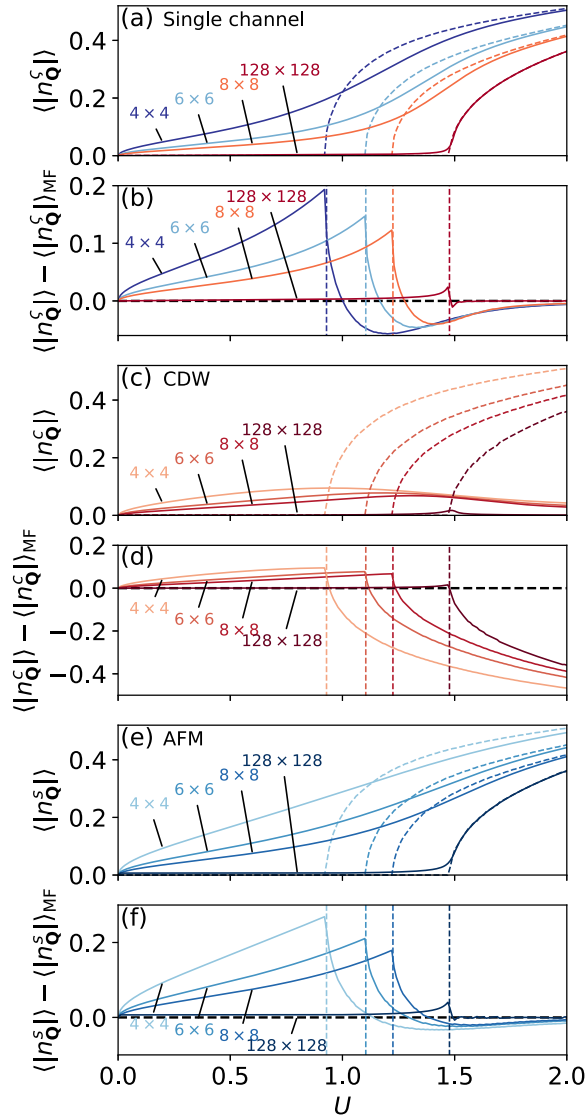

FIG. 6. The measure $\langle|n^{\varsigma}_{\mathbf{Q}}|\rangle$ of collective fluctuations is calculated along $V = U/4$ in the phase diagram for 4×4, 6×6, 8×8, and 128×128 plaquettes at $\beta = 10$ in (a), (c), and (e). Dashed lines in (a), (c), and (e) denote the saddle-point (mean-field) measure $\langle|n^{\varsigma}_{\mathbf{Q}}|\rangle_{\mathrm{MF}}$. In (b), (d), and (f), the difference $\langle|n^{\varsigma}_{\mathbf{Q}}|\rangle - \langle|n^{\varsigma}_{\mathbf{Q}}|\rangle_{\mathrm{MF}}$ is plotted. Dashed lines in (a), (c), and (e) denote the saddle-point estimate of the phase transition boundaries. Without interplay, displayed in (a), (b), the two modes $\varsigma = c, s$ are degenerate along $V = U/4$. With interplay, displayed in (c), (d) for the CDW mode and (e), (f) for the AFM mode, the degeneracy is broken. However, due to degeneracy of saddle-point minima of the channels, two choices of $\langle|n^{\varsigma}_{\mathbf{Q}}|\rangle_{\mathrm{MF}}$ exist: zero or nonzero.

following the saddle-point choice associated with a nonzero $\langle|n^{s}_{\mathbf{Q}}|\rangle_{\mathrm{MF}}$ and vanishing $\langle|n^{c}_{\mathbf{Q}}|\rangle_{\mathrm{MF}}$. The main message remains from the single-channel considerations—contributions from collective fluctuations around the minimum of the free energy are of largest importance near the phase boundaries evaulated within mean-field theory, with most significant contributions for small system sizes.

V. CONCLUSION

We have introduced a multichannel extension of the FF approach to address interplaying collective fluctuations for correlated electronic systems based on a variational optimization of a trial action respecting the underlying symmetries of the system. Exploiting this numerically low-cost method, we are able to study competing CDW and AFM fluctuations in the half-filled extended Hubbard model from small to large plaquettes. The MCFF method predicts a repulsive U-V phase diagram in qualitative agreement with more costly methods. Our approach correctly captures the $U \to 0$ limit for the CDW phase boundary, which is a nontrivial problem for computationally heavy cluster-based DMFT techniques due to the cluster size limitations. In addition, at intermediate interactions a first-order CDW-AFM transition $U = 4V$ is captured in agreement with numerically exact methods. A quantitative agreement is observed with respect to DCA simulations [29], with both approaches observing a coexistence region of collective AFM and CDW fluctuations. The coexistence regions display a strength of the MCFF approach, as it allows direct access to distinguish between the stable and MS phases. Studying the evolution of interplaying collective fluctuations, we observe MCFF theory to incorporate effects beyond mean-field theory which are exceptionally important for treatment in the vicinity of the phase boundaries for small plaquettes. The general nature of the MCFF theory makes it a promising tool for studying the interplay of collective fluctuations in strongly interacting electronic systems.

ACKNOWLEDGMENTS

The authors are thankful to A. Rubtsov for inspiring discussions and to M. Chatzieleftheriou, B. Douçot, and K. Le Hur for useful comments. The authors also acknowledge the help of the CPHT computer support team and support from IDRIS/GENCI Orsay under Project No. A0130901393. QMC simulations were performed on the national supercomputer HPE Apollo Hawk at the High Performance Computing Center Stuttgart (HLRS) under the Grant No. QMCdyn-COR/44167. The work of E.L. was supported by funding from the doctoral school of Institut Polytechnique de Paris. The work of E.A.S was supported by the European Union's Horizon 2020 Research and Innovation program under Marie Skłodowska Curie Grant Agreement No. 839551–2DMAGICS.

APPENDIX A: VARIATIONAL PRINCIPLE

In this Appendix, we present a detailed derivation of the stiffness constant $J^\varsigma_{\mathbf{Q}}$. To this aim, we apply the Peierls-Feynman-Bogoliubov variational principle that maps the initial problem Eq. (2) on the trial action Eq. (7) by minimizing the free energy $\mathcal{F}(J^\varsigma_{\mathbf{Q}})$ Eq. (6) with respect to variations in $J^\varsigma_{\mathbf{Q}}$. The free energy can be explicitly rewritten as

$$\mathcal{F}(J^\varsigma_{\mathbf{Q}}) = \mathcal{F}_c(J^\varsigma_{\mathbf{Q}}) + \frac{1}{\beta N}\left\langle \frac{U}{\beta N}\sum_{\mathbf{q},\omega}\rho_{\mathbf{q}\omega\uparrow}\rho_{-\mathbf{q},-\omega\downarrow} + \frac{1}{2}\sum_{\mathbf{q},\omega}\frac{V_{\mathbf{q}}}{\beta N}\rho_{\mathbf{q}\omega}\rho_{-\mathbf{q},-\omega} - \sum_{\varsigma}\frac{1}{2}\frac{J^\varsigma_{\mathbf{Q}}}{\beta N}\rho^\varsigma_{\mathbf{Q}}\rho^\varsigma_{-\mathbf{Q}}\right\rangle_{\mathcal{S}_c}. \tag{A1}$$

Now exploiting Eq. (8), we may rewrite the local interaction term explicitly using Wick's theorem as

$$\begin{aligned} U\langle n_{j\tau\uparrow}n_{j\tau\downarrow}\rangle_{\mathcal{S}_c} &= U\langle\langle c^\dagger_{j\tau\uparrow}c_{j\tau\uparrow}c^\dagger_{j\tau\downarrow}c_{j\tau\downarrow}\rangle_{\mathcal{S}_e}\rangle_{\mathcal{S}_\phi} = U\langle\langle c^\dagger_{j\tau\uparrow}c_{j\tau\uparrow}\rangle_{\mathcal{S}_e}\langle c^\dagger_{j\tau\downarrow}c_{j\tau\downarrow}\rangle_{\mathcal{S}_e} - \langle c^\dagger_{j\tau\uparrow}c_{j\tau\downarrow}\rangle_{\mathcal{S}_e}\langle c^\dagger_{j\tau\downarrow}c_{j\tau\uparrow}\rangle_{\mathcal{S}_e}\rangle_{\mathcal{S}_\phi} \\ &= \frac{U}{4}\left\langle\left\langle n^c_{j\tau}\right\rangle^2_{\mathcal{S}_e} - \left\langle \vec{n}^s_{j\tau}\right\rangle^2_{\mathcal{S}_e}\right\rangle_{\mathcal{S}_\phi}, \end{aligned} \tag{A2}$$

where, for convenience, we have employed a real-space representation for the interaction term. Rewriting the term in the Fourier basis, we arrive at

$$\sum_{j,\tau}U\langle\rho_{j\tau\uparrow}\rho_{j\tau\downarrow}\rangle_{\mathcal{S}_c} = \frac{1}{\beta N}\sum_{\mathbf{q},\omega}\frac{U}{4}\left\langle\left\langle\rho^c_{\mathbf{q}\omega}\right\rangle_{\mathcal{S}_e}\cdot\left\langle\rho^c_{-\mathbf{q},-\omega}\right\rangle_{\mathcal{S}_e} - \left\langle\vec{\rho}^s_{\mathbf{q}\omega}\right\rangle_{\mathcal{S}_e}\cdot\left\langle\vec{\rho}^s_{-\mathbf{q},-\omega}\right\rangle_{\mathcal{S}_e}\right\rangle_{\mathcal{S}_\phi}. \tag{A3}$$

Similarly, we may rewrite the nonlocal interaction term approximately using Wick's theorem as

$$\begin{aligned} \frac{1}{2}V_{ij}\langle n_{i\tau}n_{j\tau}\rangle_{\mathcal{S}_c} &= \frac{1}{2}V_{ij}\sum_{\sigma\sigma'}\langle\langle c^\dagger_{i\tau\sigma}c_{i\tau\sigma}c^\dagger_{j\tau\sigma'}c_{j\tau\sigma'}\rangle_{\mathcal{S}_e}\rangle_{\mathcal{S}_\phi} = \frac{1}{2}V_{ij}\sum_{\sigma\sigma'}\langle\langle c^\dagger_{i\tau\sigma}c_{i\tau\sigma}\rangle_{\mathcal{S}_e}\langle c^\dagger_{j\tau\sigma'}c_{j\tau\sigma'}\rangle_{\mathcal{S}_e} - \langle c^\dagger_{i\tau\sigma}c_{j\tau\sigma'}\rangle_{\mathcal{S}_e}\langle c^\dagger_{j\tau\sigma'}c_{i\tau\sigma}\rangle_{\mathcal{S}_e}\rangle_{\mathcal{S}_\phi} \\ &\approx \frac{1}{2}V_{ij}\left\langle\left\langle n^c_{i\tau}\right\rangle_{\mathcal{S}_e}\left\langle n^c_{j\tau}\right\rangle_{\mathcal{S}_e}\right\rangle_{\mathcal{S}_\phi}, \end{aligned} \tag{A4}$$

where $i \neq j$. Note that on the last line of this equation we have dropped the subleading nonlocal expectation values scaling as $1/N$, see Ref. [71]. Rewriting the term in the Fourier basis, we arrive at

$$\frac{1}{2}\sum_{ij,\tau}V_{ij}\langle\rho_{i\tau}\rho_{j\tau}\rangle_{\mathcal{S}_c} \approx \frac{1}{2\beta N}\sum_{\mathbf{q},\omega}V_{\mathbf{q}}\left\langle\left\langle\rho^c_{\mathbf{q}\omega}\right\rangle_{\mathcal{S}_e}\left\langle\rho^c_{-\mathbf{q},-\omega}\right\rangle_{\mathcal{S}_e}\right\rangle_{\mathcal{S}_\phi}. \tag{A5}$$

Similarly, we approximately evaluate the expectation value of the interaction in the MCFF action as

$$\frac{1}{2}\frac{J^\varsigma_{\mathbf{Q}}}{\beta N}\langle\rho^\varsigma_{\mathbf{Q}}\rho^\varsigma_{-\mathbf{Q}}\rangle_{\mathcal{S}_c} \approx \frac{1}{2}\frac{J^\varsigma_{\mathbf{Q}}}{\beta N}\left\langle\left\langle\rho^\varsigma_{\mathbf{Q}}\right\rangle_{\mathcal{S}_e}\left\langle\rho^\varsigma_{-\mathbf{Q}}\right\rangle_{\mathcal{S}_e}\right\rangle_{\mathcal{S}_\phi}. \tag{A6}$$

The form of the MCFF action $\mathcal{S}_e$ Eq. (9) only allows for certain quasimomentum modes of the local and nonlocal interaction terms to contribute to the free energy. Specifically, only the static ($\omega = 0$) component with the momentum $\mathbf{q} = \mathbf{Q}$ contributes to the average of the shifted density: $\langle \rho^\varsigma_{\mathbf{q}\omega} \rangle_{\mathcal{S}_c} = \langle \rho^\varsigma_{\mathbf{Q}} \rangle_{\mathcal{S}_c}$. Thus, the free energy Eq. (A1) takes the following form:

$$\mathcal{F}(J^\varsigma_{\mathbf{Q}}) \approx \mathcal{F}_c(J^\varsigma_{\mathbf{Q}}) + \frac{1}{(\beta N)^2}\left(\frac{U}{4} + \frac{V_{\mathbf{Q}}}{2} - \frac{J^c_{\mathbf{Q}}}{2}\right)\langle\langle \rho^c_{\mathbf{Q}}\rangle_{\mathcal{S}_e}\langle \rho^c_{-\mathbf{Q}}\rangle_{\mathcal{S}_e}\rangle_{\mathcal{S}_\phi} - \frac{1}{(\beta N)^2}\left(\frac{U}{4} + \frac{J^s_{\mathbf{Q}}}{2}\right)\langle\langle \vec{\rho}^s_{\mathbf{Q}}\rangle_{\mathcal{S}_e}\langle \vec{\rho}^s_{-\mathbf{Q}}\rangle_{\mathcal{S}_e}\rangle_{\mathcal{S}_\phi}. \tag{A7}$$

The stiffnesses $J^\varsigma_{\mathbf{Q}}$ may now be constructed by the proposed variational approach by varying the free energy $\mathcal{F}(J^\varsigma_{\mathbf{Q}})$ with respect to $J^\varsigma_{\mathbf{Q}}$, i.e., $\partial\mathcal{F}/\partial J^\varsigma_{\mathbf{Q}} = 0$. We thus identify $J^s_{\mathbf{Q}} = -\frac{U}{2}$ and $J^c_{\mathbf{Q}} = \frac{U}{2} + V_{\mathbf{Q}}$. This completes the determination of the stiffness constants $J^\varsigma_{\mathbf{Q}}$.

APPENDIX B: PHASE BOUNDARIES WITHIN THE SINGLE-CHANNEL FLUCTUATING FIELD APPROACH

In this Appendix, a derivation of the CDW and AFM phase boundaries within the single-channel FF theory, i.e., without interplaying collective fluctuations, is given. We begin by limiting our considerations to a single classical field, either in the CDW channel ($\phi^c_{\mathbf{Q}}$) or in the AFM channel ($\phi^s_{\mathbf{Q}}$). This is valid in the weak-coupling regime, where the competition between the two channels is not strong. An effective action $\mathcal{S}_{\phi^\varsigma}$ can be constructed as in Eq. (5), limited to the single $\phi^\varsigma_{\mathbf{Q}}$ mode:

$$\mathcal{S}_{\phi^\varsigma} \equiv -\mathrm{Tr}\ln\left[\mathcal{G}^{-1}_{\mathbf{k}\nu}\delta_{\mathbf{Q},0}\delta_{\sigma,\sigma'} - \phi^\varsigma_{\mathbf{Q}}\sigma^\varsigma_{\sigma\sigma'}\right] - \frac{1}{2}\frac{\beta N}{J^\varsigma_{\mathbf{Q}}}{\phi^\varsigma_{\mathbf{Q}}}^2. \tag{B1}$$

As a reminder, in this expression the trace is taken over the momenta $\mathbf{k}$, $\mathbf{Q}$, frequency ν, and spin σ, σ' indices. Considering the system at half filling ($\mu = 0$), we may explicitly sum over the momenta $\mathbf{Q}$, frequency ν, and spin σ, σ' indices in Eq. (B1), obtaining the following:

$$\mathcal{S}_{\phi^\varsigma} = -\sum_k [\ln(1 + e^{-\beta\epsilon_{\mathbf{k},+}}) + \ln(1 + e^{-\beta\epsilon_{\mathbf{k},-}})] - \frac{1}{2}\frac{\beta N}{J^\varsigma_{\mathbf{Q}}}{\phi^\varsigma_{\mathbf{Q}}}^2, \tag{B2}$$

where we have introduced the parameters $\epsilon_{\mathbf{k},\pm} = \frac{\epsilon_{\mathbf{k}}+\epsilon_{\mathbf{k}+\mathbf{Q}}}{2} \pm \sqrt{(\frac{\epsilon_{\mathbf{k}}-\epsilon_{\mathbf{k}+\mathbf{Q}}}{2})^2 + {\phi^\varsigma_{\mathbf{Q}}}^2}$ and dropped the irrelevant constant term. To identify the value of the stiffness parameter generating a phase transition, we perform a Taylor expansion for the first term of Eq. (B2), which leads to

$$\mathcal{S}_{\phi^\varsigma} = \left\{\beta\sum_k\left[\frac{f(\epsilon_{\mathbf{k}}) - f(\epsilon_{\mathbf{k}+\mathbf{Q}})}{\epsilon_{\mathbf{k}} - \epsilon_{\mathbf{k}+\mathbf{Q}}}\right] - \frac{1}{2}\frac{\beta N}{J^c_{\mathbf{Q}}}\right\}{\phi^\varsigma_{\mathbf{Q}}}^2 + O({\phi^\varsigma_{\mathbf{Q}}}^4), \tag{B3}$$

where the Fermi-Dirac distribution $f(\epsilon) \equiv 1/(e^{\beta\epsilon} + 1)$ is employed and the irrelevant constant term dropped, as previously. Thus, the phase transition can be identified by the factor associated with the ${\phi^\varsigma_{\mathbf{Q}}}^2$ term switching sign. This leads to the critical stiffness parameter for both the CDW and AFM channels to have the following analytic form:

$$J^\varsigma_{\mathbf{Q}} = 1/\Pi_{\mathbf{Q}}. \tag{B4}$$

Here, we have introduced the (static) noninteracting polarization $\Pi_{\mathbf{Q}}$, which is of a Lindhard function form:

$$\Pi_{\mathbf{Q}} \equiv \frac{2}{N}\sum_k\left[\frac{f(\epsilon_{\mathbf{k}}) - f(\epsilon_{\mathbf{k}+\mathbf{Q}})}{\epsilon_{\mathbf{k}} - \epsilon_{\mathbf{k}+\mathbf{Q}}}\right]. \tag{B5}$$

This result allows us to connect the single-channel FF calculations to the RPA and FLEX estimates of the associate phase boundaries.

The RPA estimate $V^{\mathrm{CDW}}_{U=0}$ for the CDW phase boundary and the FLEX estimate $U^{\mathrm{AFM}}_{V=0}$ for the AFM phase boundary can be obtained as follows. The CDW phase boundary is identified by a divergence of the charge susceptibility of RPA at the $\mathbf{Q} = (\pi, \pi)$ points. At $U = 0$ this divergence arises if the condition $1 - \Pi_{\mathbf{Q}}V_{\mathbf{Q}} = 0$ is satisfied. This gives the following estimate for the CDW phase boundary:

$$V_{\mathbf{Q}} = 1/\Pi_{\mathbf{Q}}. \tag{B6}$$

Analogously, the AFM phase boundary is identified by a divergence of the spin susceptibility at the $\mathbf{Q} = (\pi, \pi)$ point. Using the FLEX form for the bare local spin interaction $U^s = -U/2$ leads to the following condition for identifying the AFM phase boundary: $1 - U^s\Pi_{\mathbf{Q}} = 0$ or, equivalently, to

$$U^s = 1/\Pi_{\mathbf{Q}}. \tag{B7}$$

These results show that the single-channel FF theory gives exactly the same estimates for the $V^{\mathrm{CDW}}_{U=0}$ and $U^{\mathrm{AFM}}_{V=0}$ transition points as RPA and FLEX, respectively. However, we emphasize that in the multichannel FF approach the $\mathrm{Tr}\ln[\cdots]$ term of the effective action Eq. (5) couples together different collective fluctuations. This means a simple analytic treatment performed above is, in general, unfeasible in the case of interplaying collective fluctuations.

[1] C. Lanczos, An iteration method for the solution of the eigenvalue problem of linear differential and integral operators, J. Res. Natl. Bur. Stand. **45**, 255 (1950).

[2] J. E. Hirsch and R. M. Fye, Monte Carlo Method for Magnetic Impurities in Metals, Phys. Rev. Lett. **56**, 2521 (1986).

[3] M. Salmhofer, C. Honerkamp, W. Metzner, and O. Lauscher, Renormalization group flows into phases with broken symmetry, Prog. Theor. Phys. **112**, 943 (2004).

[4] P. Lykos and G. W. Pratt, Discussion on the Hartree-Fock approximation, Rev. Mod. Phys. **35**, 496 (1963).

[5] J. Hubbard, Electron correlations in narrow energy bands, Proc. R. Soc. London A **276**, 238 (1963).

[6] M. C. Gutzwiller, Effect of Correlation on the Ferromagnetism of Transition Metals, Phys. Rev. Lett. **10**, 159 (1963).

[7] J. Kanamori, Electron correlation and ferromagnetism of transition metals, Prog. Theor. Phys. **30**, 275 (1963).

[8] J. Hubbard, Electron correlations in narrow energy bands. III. An improved solution, Proc. R. Soc. London A **281**, 401 (1964).

[9] A. B. Harris and R. V. Lange, Single-particle excitations in narrow energy bands, Phys. Rev. **157**, 295 (1967).

[10] R. A. Bari, Effects of short-range interactions on electron-charge ordering and lattice distortions in the localized state, Phys. Rev. B **3**, 2662 (1971).

[11] S. V. Vonsovsky and M. I. Katsnelson, Some types of instabilities in the electron energy spectrum of the polar model of the crystal. I. The maximum-polarity state, J. Phys. C: Solid State Phys. **12**, 2043 (1979).

[12] V. J. Emery, Theory of the quasi-one-dimensional electron gas with strong "on-site" interactions, Phys. Rev. B **14**, 2989 (1976).

[13] J. Sólyom, The Fermi gas model of one-dimensional conductors, Adv. Phys. **28**, 201 (1979).

[14] V. J. Emery, Theory of the One-Dimensional Electron Gas, in *Highly Conducting One-Dimensional Solids*, edited by Jozef T. Devreese, Roger P. Evrard, and Victor E. van Doren (Springer US, Boston, MA, 1979), p. 247.

[15] B. Fourcade and G. Spronken, Real-space scaling methods applied to the one-dimensional extended Hubbard model. II. The finite-cell scaling method, Phys. Rev. B **29**, 5096 (1984).

[16] J. E. Hirsch, Charge-Density-Wave to Spin-Density-Wave Transition in the Extended Hubbard Model, Phys. Rev. Lett. **53**, 2327 (1984).

[17] M. Nakamura, Mechanism of CDW-SDW transition in one dimension, J. Phys. Soc. Jpn. **68**, 3123 (1999).

[18] M. Nakamura, Tricritical behavior in the extended Hubbard chains, Phys. Rev. B **61**, 16377 (2000).

[19] M. Fabrizio, A. O. Gogolin, and A. A. Nersesyan, From Band Insulator to Mott Insulator in One Dimension, Phys. Rev. Lett. **83**, 2014 (1999).

[20] S. R. Manmana, V. Meden, R. M. Noack, and K. Schönhammer, Quantum critical behavior of the one-dimensional ionic Hubbard model, Phys. Rev. B **70**, 155115 (2004).

[21] M. Hafez Torbati, Nils A. Drescher, and Götz S. Uhrig, Dispersive excitations in one-dimensional ionic Hubbard model, Phys. Rev. B **89**, 245126 (2014).

[22] M. Hafez-Torbati and G. S. Uhrig, Orientational bond and Néel order in the two-dimensional ionic Hubbard model, Phys. Rev. B **93**, 195128 (2016).

[23] B. Fourcade and G. Spronken, Real-space scaling methods applied to the one-dimensional extended Hubbard model. I. The real-space renormalization-group method, Phys. Rev. B **29**, 5089 (1984).

[24] Y. Zhang and J. Callaway, Extended Hubbard model in two dimensions, Phys. Rev. B **39**, 9397 (1989).

[25] J. Callaway, D. P. Chen, D. G. Kanhere, and Q. Li, Small-cluster calculations for the simple and extended Hubbard models, Phys. Rev. B **42**, 465 (1990).

[26] X.-Z. Yan, Theory of the extended Hubbard model at half filling, Phys. Rev. B **48**, 7140 (1993).

[27] M. Aichhorn, H. G. Evertz, W. von der Linden, and M. Potthoff, Charge ordering in extended Hubbard models: Variational cluster approach, Phys. Rev. B **70**, 235107 (2004).

[28] B. Davoudi and A.-M. S. Tremblay, Nearest-neighbor repulsion and competing charge and spin order in the extended Hubbard model, Phys. Rev. B **74**, 035113 (2006).

[29] J. Paki, H. Terletska, S. Iskakov, and E. Gull, Charge order and antiferromagnetism in the extended Hubbard model, Phys. Rev. B **99**, 245146 (2019).

[30] P. Pudleiner, A. Kauch, K. Held, and G. Li, Competition between antiferromagnetic and charge density wave fluctuations in the extended Hubbard model, Phys. Rev. B **100**, 075108 (2019).

[31] E. A. Stepanov, V. Harkov, M. Rösner, A. I. Lichtenstein, M. I. Katsnelson, and A. N. Rudenko, Coexisting charge density wave and ferromagnetic instabilities in monolayer InSe, npj Comput. Mater. **8**, 118 (2022).

[32] M. Vandelli, A. Galler, A. Rubio, A. I. Lichtenstein, S. Biermann, and E. A. Stepanov, Doping-dependent charge- and spin-density wave orderings in a monolayer of Pb adatoms on Si(111), arXiv:2301.07162.

[33] T. Ayral, S. Biermann, and P. Werner, Screening and nonlocal correlations in the extended Hubbard model from self-consistent combined *GW* and dynamical mean field theory, Phys. Rev. B **87**, 125149 (2013).

[34] H. Hafermann, E. G. C. P. van Loon, M. I. Katsnelson, A. I. Lichtenstein, and O. Parcollet, Collective charge excitations of strongly correlated electrons, vertex corrections, and gauge invariance, Phys. Rev. B **90**, 235105 (2014).

[35] H. Terletska, T. Chen, and E. Gull, Charge ordering and correlation effects in the extended Hubbard model, Phys. Rev. B **95**, 115149 (2017).

[36] E. G. C. P. van Loon and M. I. Katsnelson, The extended Hubbard model with attractive interactions, J. Phys.: Conf. Ser. **1136**, 012006 (2018).

[37] A. A. Katanin, Extended dynamical mean field theory combined with the two-particle irreducible functional renormalization-group approach as a tool to study strongly correlated systems, Phys. Rev. B **99**, 115112 (2019).

[38] M. Vandelli, V. Harkov, E. A. Stepanov, J. Gukelberger, E. Kozik, A. Rubio, and A. I. Lichtenstein, Dual boson diagrammatic Monte Carlo approach applied to the extended Hubbard model, Phys. Rev. B **102**, 195109 (2020).

[39] H. Terletska, S. Iskakov, T. Maier, and E. Gull, Dynamical cluster approximation study of electron localization in the extended Hubbard model, Phys. Rev. B **104**, 085129 (2021).

[40] E. A. Stepanov, A. Huber, E. G. C. P. van Loon, A. I. Lichtenstein, and M. I. Katsnelson, From local to nonlocal correlations: The Dual Boson perspective, Phys. Rev. B **94**, 205110 (2016).

[41] E. A. Stepanov, A. Huber, A. I. Lichtenstein, and M. I. Katsnelson, Effective Ising model for correlated systems with charge ordering, Phys. Rev. B **99**, 115124 (2019).

[42] A.M. Oleś, R. Micnas, S. Robaszkiewicz, and K.A. Chao, Ground state of the half-filled extended Hubbard model beyond the Hartree-Fock approximation, Phys. Lett. A **102**, 323 (1984).

[43] M. H. Hettler, A. N. Tahvildar-Zadeh, M. Jarrell, T. Pruschke, and H. R. Krishnamurthy, Nonlocal dynamical correlations of strongly interacting electron systems, Phys. Rev. B **58**, R7475 (1998).

[44] M. H. Hettler, M. Mukherjee, M. Jarrell, and H. R. Krishnamurthy, Dynamical cluster approximation: Nonlocal dynamics of correlated electron systems, Phys. Rev. B **61**, 12739 (2000).

[45] K. Aryanpour, M. H. Hettler, and M. Jarrell, Analysis of the dynamical cluster approximation for the Hubbard model, Phys. Rev. B **65**, 153102 (2002).
[46] P. C. Hohenberg, Existence of long-range order in one and two dimensions, Phys. Rev. **158**, 383 (1967).
[47] N. D. Mermin and H. Wagner, Absence of ferromagnetism or antiferromagnetism in one- or two-dimensional isotropic Heisenberg models, Phys. Rev. Lett. **17**, 1133 (1966).
[48] M. B. Walker and Th. W. Ruijgrok, Absence of magnetic ordering in one and two dimensions in a many-band model for interacting electrons in a metal, Phys. Rev. **171**, 513 (1968).
[49] A. I. Lichtenstein and M. I. Katsnelson, Antiferromagnetism and *d*-wave superconductivity in cuprates: A cluster dynamical mean-field theory, Phys. Rev. B **62**, R9283 (2000).
[50] G. Kotliar, S. Y. Savrasov, G. Pálsson, and G. Biroli, Cellular dynamical mean field approach to strongly correlated systems, Phys. Rev. Lett. **87**, 186401 (2001).
[51] T. Maier, M. Jarrell, T. Pruschke, and M. H. Hettler, Quantum cluster theories, Rev. Mod. Phys. **77**, 1027 (2005).
[52] A.-M. S. Tremblay, B. Kyung, and D. Sénéchal, Pseudogap and high-temperature superconductivity from weak to strong coupling. Towards a quantitative theory, Low Temp. Phys. **32**, 424 (2006).
[53] G. Kotliar, S. Y. Savrasov, K. Haule, V. S. Oudovenko, O. Parcollet, and C. A. Marianetti, Electronic structure calculations with dynamical mean-field theory, Rev. Mod. Phys. **78**, 865 (2006).
[54] M. Harland, M. I. Katsnelson, and A. I. Lichtenstein, Plaquette valence bond theory of high-temperature superconductivity, Phys. Rev. B **94**, 125133 (2016).
[55] I. T. Diatlov, V. V. Sudakov, and K. A. Ter-Martirosian, Asymptotic meson-meson scattering theory, Sov. Phys. JETP **5**, 631 (1957).
[56] C. De Dominicis, Variational formulations of equilibrium statistical mechanics, J. Math. Phys. **3**, 983 (1962).
[57] C. De Dominicis, Stationary entropy principle and renormalization in normal and superfluid systems. I. Algebraic formulation, J. Math. Phys. **5**, 14 (1964).
[58] N. E. Bickers and D. J. Scalapino, Conserving approximations for strongly fluctuating electron systems. I. Formalism and calculational approach, Ann. Phys. **193**, 206 (1989).
[59] N. E. Bickers and S. R. White, Conserving approximations for strongly fluctuating electron systems. II. numerical results and parquet extension, Phys. Rev. B **43**, 8044 (1991).
[60] N. E. Bickers, Self-consistent many-body theory for condensed matter systems, *Theoretical Methods for Strongly Correlated Electrons* (Springer, New York, 2004), p. 237.
[61] G. Rohringer, H. Hafermann, A. Toschi, A. A. Katanin, A. E. Antipov, M. I. Katsnelson, A. I. Lichtenstein, A. N. Rubtsov, and K. Held, Diagrammatic routes to nonlocal correlations beyond dynamical mean field theory, Rev. Mod. Phys. **90**, 025003 (2018).
[62] E. G. C. P. van Loon, A. I. Lichtenstein, M. I. Katsnelson, O. Parcollet, and H. Hafermann, Beyond extended dynamical mean-field theory: Dual boson approach to the two-dimensional extended Hubbard model, Phys. Rev. B **90**, 235135 (2014).
[63] E. A. Stepanov, E. G. C. P. van Loon, A. A. Katanin, A. I. Lichtenstein, M. I. Katsnelson, and A. N. Rubtsov, Self-consistent dual boson approach to single-particle and collective excitations in correlated systems, Phys. Rev. B **93**, 045107 (2016).
[64] L. Peters, E. G. C. P. van Loon, A. N. Rubtsov, A. I. Lichtenstein, M. I. Katsnelson, and E. A. Stepanov, Dual boson approach with instantaneous interaction, Phys. Rev. B **100**, 165128 (2019).
[65] A. Galler, P. Thunström, P. Gunacker, J. M. Tomczak, and K. Held, *Ab initio* dynamical vertex approximation, Phys. Rev. B **95**, 115107 (2017).
[66] A. Galler, J. Kaufmann, P. Gunacker, M. Pickem, P. Thunström, J. M. Tomczak, and K. Held, Towards *ab initio* calculations with the dynamical vertex approximation, J. Phys. Soc. Jpn. **87**, 041004 (2018).
[67] X. Cao, T. Ayral, Z. Zhong, O. Parcollet, D. Manske, and P. Hansmann, Chiral *d*-wave superconductivity in a triangular surface lattice mediated by long-range interaction, Phys. Rev. B **97**, 155145 (2018).
[68] M. Vandelli, J. Kaufmann, M. El-Nabulsi, V. Harkov, A. I. Lichtenstein, and E. A. Stepanov, Multi-band D-TRILEX approach to materials with strong electronic correlations, SciPost Phys. **13**, 036 (2022).
[69] A. N. Rubtsov, Fluctuating local field method probed for a description of small classical correlated lattices, Phys. Rev. E **97**, 052120 (2018).
[70] D. Kuznetsova, G. V. Astretsov, and A. N. Rubtsov, Fluctuating local field method for the disordered Ising model, arXiv:2212.14733.
[71] A. N. Rubtsov, E. A. Stepanov, and A. I. Lichtenstein, Collective magnetic fluctuations in Hubbard plaquettes captured by fluctuating local field method, Phys. Rev. B **102**, 224423 (2020).
[72] Y. S. Lyakhova, E. A. Stepanov, and A. N. Rubtsov, Fluctuating local field approach to free energy of one-dimensional molecules with strong collective electronic fluctuations, Phys. Rev. B **105**, 035118 (2022).
[73] Y. S. Lyakhova and A. N. Rubtsov, Fluctuating local field approach to the description of lattice models in the strong coupling regime, J. Supercond. Nov. Magn. **35**, 2169 (2022).
[74] E. Coronado, Molecular magnetism: from chemical design to spin control in molecules, materials and devices, Nat. Phys. **5**, 87 (2020).
[75] P. Fazekas, *Lecture Notes on Electron Correlation and Magnetism* (World Scientific, Singapore, 1999).
[76] M. Holynska, *Single-Molecule Magnets: Molecular Architectures and Building Blocks for Spintronics* (John Wiley & Sons, New York, 2019).
[77] M. Schüler, M. Rösner, T. O. Wehling, A. I. Lichtenstein, and M. I. Katsnelson, Optimal Hubbard Models for Materials with Nonlocal Coulomb Interactions: Graphene, Silicene, and Benzene, Phys. Rev. Lett. **111**, 036601 (2013).
[78] T. Ayral, S. Biermann, P. Werner, and L. Boehnke, Influence of Fock exchange in combined many-body perturbation and dynamical mean field theory, Phys. Rev. B **95**, 245130 (2017).
[79] R. Peierls, On a minimum property of the free energy, Phys. Rev. **54**, 918 (1938).
[80] N. N. Bogolyubov, A variation principle in the problem of many bodies, Dokl. Akad. Nauk SSSR (Russian Academy of Sciences) **119**, 244 (1958).

[81] R. P. Feynman, *Statistical Mechanics: A Set of Lectures* (Benjamin/Cummings, Reading, MA, 1972).

[82] J. Jaeckel and C. Wetterich, Flow equations without mean field ambiguity, Phys. Rev. D **68**, 025020 (2003).

[83] T. Baier, E. Bick, and C. Wetterich, Temperature dependence of antiferromagnetic order in the Hubbard model, Phys. Rev. B **70**, 125111 (2004).

[84] J. Jaeckel, Understanding the Fierz ambiguity of partially bosonized theories, arXiv:hep-ph/0205154.

[85] L. Philoxene, V. H. Dao, and R. Frésard, Spin and charge modulations of a half-filled extended Hubbard model, Phys. Rev. B **106**, 235131 (2022).

[86] E. A. Stepanov, V. Harkov, and A. I. Lichtenstein, Consistent partial bosonization of the extended Hubbard model, Phys. Rev. B **100**, 205115 (2019).

[87] V. Harkov, M. Vandelli, S. Brener, A. I. Lichtenstein, and E. A. Stepanov, Impact of partially bosonized collective fluctuations on electronic degrees of freedom, Phys. Rev. B **103**, 245123 (2021).

[88] F. Šimkovic, J. P. F. LeBlanc, A. J. Kim, Y. Deng, N. V. Prokof'ev, B. V. Svistunov, and E. Kozik, Extended Crossover from a Fermi Liquid to a Quasiantiferromagnet in the Half-Filled 2D Hubbard Model, Phys. Rev. Lett. **124**, 017003 (2020).

[89] J. R. Engelbrecht, M. Randeria, and C. A. R. Sá de Melo, BCS to Bose crossover: Broken-symmetry state, Phys. Rev. B **55**, 15153 (1997).

[90] S. N. Klimin, J. Tempere, T. Repplinger, and H. Kurkjian, Collective excitations of a charged Fermi superfluid in the BCS-BEC crossover, New J. Phys. **25**, 063011 (2023).